Proceedings of OMAE2006
25th International Conference on Offshore Mechanics and Arctic Engineering
June 4-9, 2006, Hamburg, Germany

OMAE2006-92673

TRUSS SPAR VORTEX INDUCED MOTIONS: BENCHMARKING OF CFD AND MODEL TESTS

John Halkyard
Technip USA, Houston, Texas

Sampath Atluri
Technip USA, Houston, Texas

Senu Sirnivas
Technip USA, Houston, Texas

ABSTRACT

Spar production systems are subject to Vortex Induced Motions (VIM) which may impact mooring and riser design. Helical strakes are employed to mitigate VIM. Model tests are typically required to validate the performance of the strakes. This paper will report on the results of benchmarking studies that have been conducted over the past few years to compare model tests with computational fluid dynamics (CFD). The paper discusses comparisons of CFD with model tests, "best practices" for the use of CFD for these classes of problems and issues related to turbulence modeling and meshing of problems at large Reynold's numbers. This work is ongoing.

INTRODUCTION

Fourteen spar production platforms have been installed in the deepwater Gulf of Mexico. The first was the Oryx (now Kerr McGee) Neptune Spar in 1996. The latest is the Kerr McGee Constitution Spar. The spar is a bluff, vertical cylinder which is subject to Vortex Induced Motions (VIM) when current velocities exceed a few knots, or less in ultra-deep water. All of the spars have been constructed with helical strakes to mitigate VIM. Model tests have indicated that the effectiveness of these strakes is influenced greatly by details of their design such as appurtenances placed on the outside of the hull, discontinuities in the strake layout, and holes in the strakes. Because of the low aspect ratio of the spar displacement hull (hard tank), the effectiveness of the strakes is not omni-directional: responses show distinct “hot spots” for certain current directions. The authors have been investigating the use of CFD as a means for predicting VIM performance and for facilitating the design of spars for reduced VIM. The motivation for this is the reduction in time and costs associated with model tests which invariably are required if Spar VIM is a factor in the design of the spar or mooring system.

Three classic spars currently are in use. They are circular cylinders, approximately 700 ft long with diameters of 72 and 122 ft. The truss spars are similar in overall dimensions, but the circular cylinder is truncated and the lower part of the hull consists of an open truss structure. The cell spar is the newest generation of spar platform. It consists of a cluster of smaller cylinders. In all cases the spars float vertically, and are held in place by mooring lines which are attached close to mid-draft of the hull. More details on these spar design may be found in [1,2,3]. The helical strakes are typically restricted to the large diameter “hard tank” of the truss spars, but the Red Hawk cell spar also had strakes on the smaller diameter legs [3].

Spar mooring systems permit motions in six degrees of freedom: surge, sway, heave, roll, yaw and pitch, however, surge and sway are the dominant motions in current-induced VIM. Surge is assumed to correspond to be in-line with the current. VIM lock-in occurs when the reduced velocity, Urn, is in a critical range called “lock-in” [4].

$$U_{rn} = \frac{uT_n}{D} \qquad (1)$$

Tn is the natural period of the spar in calm water with no current. In lock-in the sway motion (transverse to the current) of a cylinder oscillates with a period close to Tn, and with an amplitude that can approach the spar diameter. Mean drag increases proportional to the amplitude of this motion.

Appurtenances and geometric variations may result in a significant deterioration in the performance of the strakes which has been well documented [5-8]. If the mooring system design is controlled by the spar’s response in currents, the amplitude of VIM and the associated drag enhancement could be the most important determinant in the design of the mooring system.

There is presently no generally accepted analytical method for predicting the VIM behavior of spar platforms. Model tests are

required to obtain the necessary design data. These tests are costly and require a long lead time. If modeling and meshing is automated, CFD can produce results in days whereas tests take several weeks to plan and implement. The purpose of the research described in this paper is to determine whether CFD can be used as a proxy for model tests, if not for the final design, at least to perform optimization studies at an early stage of the design. The current research has the goal of benchmarking CFD against model tests to provide suitable confidence in the results. We are also investigating appropriate practices in meshing and modeling to provide "best practices" for the implementation of CFD into the design process

We have reported previously on model tests for a three-start strake configuration and comparisons with CFD results [9]. Further CFD runs applied to this data set are described in [10]. In what follows we first describe a set of model tests on a truss spar for four-start strakes, and CFD benchmarking efforts to date. In this example, we have used CFD in to evaluate the impact of changing the pitch of the strakes.

NOMENCLATURE

U_{rn}= Reduced velocity based on calm water period
T_n = Natural period in calm water without current
D = Diameter of Spar hard tank

PREVIOUS RESULTS

Reference [9] describes a set of experiments and CFD results. The experimental model consisted of a hard tank cylinder with a diameter, D, equal to 0.741 m, a 1.4 m draft, and a truss section which extended the total draft to 3.8 m. The hard tank had a very small amount of roughness, estimated at k/D = .0004. Towing tests were carried out by Force Technology (formerly the Danish Maritime Institute). The model was outfitted with three-start helical strakes with a height equal to 13% of the diameter. Two different strake pitches were tested: "full strakes" spanning 120 degrees each and "overlapping strakes" spanning 150 degrees. The pitch/diameter ratios are 4.53 and 3.63, respectively. Typical ratios for longer cylinders and risers range from around five to 20. The lower values for the truss spars is required to achieve sufficient coverage on a short length of cylinder to insure that the strake causes separation of the flow.

Figure 1 shows a comparison of the model tests with CFD results for the full strake case. The experiments showed three "hot spots" in the VIM response as might be expected with three-start strakes. However, the amplitude of the hot spot peaks was not uniform. This is due in part to the asymmetry in the positioning of the mooring chain in this model, and perhaps due to the asymmetry of the truss with respect to the strakes. The CFD results shown did not include the chains and fairleads. And the truss model was a Morison approximation which was symmetric [9]. Hence, the CFD results yield exactly equal hot spots from symmetry.

CFD is accurately predicting the location of the hot spots; however it is overpredicting the peak responses at those points. Investigation of the flow patterns suggests that the hot spots are a result of the preponderance of streamlines separating from the cylinder, as opposed to the strakes themselves.

Further CFD runs have been performed to improve the predictions. We have found that more accurate geometry modeling, e.g. the chains, strake thickness and holes in the strakes can change the results. Also, meshing in the vicinity of the boundary layer is important, particularly for the case of flow separation from the cylinder. These results will be discussed [10].

FOUR-START STRAKE TESTS

The same model used for the tests described above was modified and tested with four strakes. The scale remained 1:40. The model was equipped with four strakes with a height of 13% of D. The upper start points of the strakes were 267 mm below the waterline corresponding to 35 ft in full-scale. At the lower end the strakes were shortened by 6 mm and were cut at an angle of 15° (to horizontal) to avoid interference with the mooring lines. The strakes had an angle from horizontal of 57.6°. Each strake covered 108° leaving an 18° overlap. This corresponds to a pitch/diameter ratio of 5.0. Figure 2 shows the model installed in the Force Technology towing tank.

Two configurations were tested. Configuration A included chains running the length of the hull to represent the mooring lines between the deck and the fairleads. Figure 3 shows this configuration looking up from the bottom of the hard tank. Figure 4 shows the positioning of the chains and strakes as a rollout of the hard tank. The coordinate system is shown in Figure 5.

A second configuration (B) was tested without the chains and with the corresponding holes in the strakes covered. Otherwise it is the same.

Table 1 shows the measured natural periods of the model. The same mooring system was used as in the previous tests [8,9], yet the natural surge/sway period was reduced from about 26.3 to 25.5 seconds (model scale). This suggests that the four-start strakes result in less added mass than the three start strakes.

TEST RESULTS

Measurements were made of all the degrees of freedom of the motion and the drag on the spar. Results are normalized to the spar diameter, D. We are primarily concerned with the

transverse motion (Y-direction). Figure 6 shows typical plots of the motions X/D (surge) and Y/D (sway), together with a trajectory plot of the X-Y motion. Figures 7 and 8 show the maximum standard deviations of Y/D measured in all the tests with Configuration A and B, respectively. Figure 9 shows this data consolidated in one plot. Configuration B (no appurtenances or holes in strakes) data was only collected near the hot spots. The results indicate, in this case, that the chains and holes in the strakes did not affect the responses much.

Comparing Figure 1 with Figure 7 shows, in fact, that the hot spot peaks are more pronounced with four-starts vs. three-starts.

The data is presented here as the standard deviation of the experiments. The maximum value of Y/D is sometimes defined, for a given record, as:

$$Y/D_{max} = (\text{Maximum Y/D} - \text{Minimum Y/D})/2$$

If the VIM were sinusoidal this ratio between Y/D_{max} and $Y/D_{standard\ deviation}$ would be 1.414. As seen from Figure 6, for example, the response is modulated and not uniform amplitude. The average ratio for the four-start data presented here is 2.7. The ratio for the earlier three-start tests was 2.6.

Comparing Figures 1 and 7 again, it can also be stated that the four-start strakes are not performing better than the three-start strakes. There are more hot spots with the four start strakes, and their amplitude is equal to or greater than those observed with three-starts.

It was speculated that by increasing the overlap, the four-start strake performance could be improved, just as it was for the three-start strakes [9]. One purpose of the CFD calculations discussed below was to check this hypothesis.

CFD CALCULATIONS

All of the solutions shown here were produced using AcuSolve™. AcuSolve™ is a finite element CFD solver. It is based on the Galerkin/Least Squares formulation and supports a variety of element types. AcuSolve™ uses a fully coupled pressure/velocity iterative solver plus a generalized alpha method as a semi-discrete time stepping algorithm [11]. It is second order accurate in space and time.

Turbulence was modeled using Spalart's version of detached eddy simulation (DES). This DES model is based on the one-equation turbulence model of Spalart-Allmaras [12]. Near the wall the model acts like the S-A Reynolds averaged Navier Stokes (RANS) model and far from the wall it behaves similarly to large eddy simulation (LES) models. As implemented in AcuSolve™, DES transitions smoothly from RANS to LES configurations. The constants required are not listed here but are those suggested by Spalart. It should be noted that a feature of this turbulence model is that at points away from the wall, unresolved (subgrid scale) turbulence is assumed to be isotropic and the eddy viscosity is a function of element size. A danger at the high Re of the problems solved here is that this last assumption is not met. We used wall functions to describe the flow at the wall in all CFD simulations. This was done to economize on mesh size, but also because both model tests and the full scale spar have rough surfaces.

A typical mesh used in the original simulations is reported in [9]. The fluid domain is a parallelepiped with inlet and outlet planes. The mesh is designed with small grid spacing in the wake and relatively coarse grid spacing elsewhere in to provide an economical grid. Note that the lower truss portion of the model is not modeled explicitly. Rather, we created user defined function for the motion of the spar which estimated the effects of the truss using Morison's equations [9]. The economies of omitting the truss and carefully defining the mesh allowed the use of relatively small meshes. Each grid contained approximately 520,000 nodes and 520,000 hexahedral elements. Typical run times for 2000 time steps, or about 30 vortex shedding cycles (equivalent to the length of experiments), on an 8 CPU Linux P4 cluster using a gigabit switch are on the order of 24 hours.

The original meshes were designed to place the first nodes away from the wall just above the surface roughness on the model. [The hard tank had been reused from previous tests that had large roughness pebbles attached. For these tests the roughness was removed and the surface cleaned, but it is estimated that the roughness still corresponds to a k/D of about .00004.] This type of mesh tends to produce average calculated values of y+ on the order of 20 with maximum values sometimes approaching 100, or larger than usually recommended for smooth cylinders.

Mesh sensitivity studies have shown that the original mesh density yields consistent results [10].

New meshes were regenerated for the four-start strake simulations. We have generated two meshes with different tools. Mesh A, shown in Figure 10, consists of 480,000 nodes and 2.8 million tetrahedral elements. Mesh B, shown in Figure 11, consists of 200,000 nodes and 1.18 million tetrahedral elements. Both meshes included a similar control volume to that used in the orginal CFD runs. Also, both meshes resulted in about the same number of hexahedral elements as the number of nodes. The primary difference between the meshes is the resolution in the boundary layer, and the element stretching along the strakes. Mesh A actually had a coarser mesh resolution in the boundary layer, even though it had more nodes. The reason is that the meshing tool used produced more

or less equilateral elements. This resulted in very small elements along the tip of the strakes which propogated into the external flow regime. Mesh B used another tool which allowed stretching of elements along the strake. Aspect ratios were as high as 30. Thus, even though the nodes were placed closer to the surface, this mesh resulted in many fewer nodes and elements. The runs consisted of 1000 – 0.5 second time steps. These runs were performed on a 16 node/32 cpu Opteron 64 Linux cluster with a Myrnet switch. Run times were four hours for Mesh A and two hours for Mesh B.

Figure 12 shows a close up of the two meshes close to the strakes illustrating the finer resolution close to the wall. As in the original work, the Law of the Wall was used to derive the shear stress at the boundary. "Best practices" [13] suggest that y+ values using the wall function should not exceed 100 and should generally not be less than 30. AcuSolve™ uses an alternate form of the wall function if y+ is less than 30, so the primary concern is for y+>100. In the problems run here the maximum y+ was abut 120 and 25 for Meshes A and B, respectively.

As we will see below, the results are somewhat dependent on the mesh. We believe that mesh B gives better results (certainly closer to the experiments), however more mesh sensitivity runs are required to make sure that the solution has converged. This work is ongoing.

The present model does not include the chains, fairleads or holes in strakes. The test results shown above indicate that these are not important in this case; however in general we believe it is important to include the appendages. Work underway that will be reported in [10] shows the impact of modeling of these items for the three-start configuration.

The hybrid fluid structure interaction model used to solve for the motion of the spar and avoid explicit modeling of the truss was based on a modified Morison's equation. The user function modeled the mooring system used in the tow tank explicitly.

In the simulations, the motion of the spar is calculated within each time step by first determining the integral of the surface tractions on the hard tank from the CFD solution. This is provided by the AcuSolve™ flow solution. The forces due to the mooring system are calculated from the instantaneous spar position and forces on the truss are calculated from the current velocity and kinematics of the spar with respect to the free stream current. The new position of the spar for the next time step is found by a simple integration using the trapezoidal rule. In effect, the new position of the spar is calculated using the force values at the middle of the step.

The motion of the spar within the mesh is accommodated using a specified mesh motion in which the position of each node is specified based on the spar position. This approach avoids the solution of nodal locations using an arbitrary elastic solid to represent the mesh (Arbitrary Langrangian Eulerian or ALE method) and hence solve for the new nodal locations. However, the fluid flow is calculated based on the new nodal locations as in the ALE method.

The coefficients for truss and soft tank added mass and drag were derived from formulations for fixed jacket structures in API RP2A and from previous model test programs. Sensitivity of the results to truss coefficients was examined in the previous work [9]. Also, the sensitivity to a pseudo-shear current was examined by setting U equal to zero in this equation. Future work will include explicit modeling of the truss as well.

RESULTS WITH FOUR-START STRAKES

Typical comparisons time series and X-Y plots for the experiments and corresponding CFD runs are shown in Figures 13 – 16. The CFD results shown are for Mesh B. These plots show responses for $U_{rn} = 9$. Since the tests only covered the Urn range of 7 – 10, we did not examine the transition to lock-in. Comparisons here consist of the maximum responses in that range of U_{rn}.

Figures 13 and 14 compare the results for a heading with minimal VIM, while Figures 15 and 16 compare the results at one of the hot spots. In both cases, for these examples, CFD is over predicting the responses of both the standard deviations and maximum values. The comparison for the hot spot (225 deg heading) is better. The maximum amplitude and the "banana" shape of the response curve look consistent.

Figure 17 shows the comparison of the VIM standard deviations for 0 – 90 degrees. The results with Mesh A diverge greatly from the experimental results at 45 and 60 degrees. The results with Mesh B diverge a bit at 0 – 30 degrees, but in general track the directional trend and amplitudes better than mesh A. We ascribe this behavior to the meshing density in the boundary layer which captures the separation of flow from the cylinder better. To the extent that flow is separating from the cylinder, as opposed to the strakes, the challenge of CFD is to accurately predict the separation point and the energy transfer into the wake vortex.

Figure 18 shows the same comparisons for the maximum values of Y/D. The same trends occur. The CFD prediction for the peak response at 60 degrees is closer in this case.

As stated above, further mesh sensitivity studies are underway to improve these correlations.

The above results are for 18 degree strake overlap. The earlier tests indicate that more strake overlap, i.e. lower pitch, might improve the results. The theory of this is that the overlapping

strakes will provide fuller coverage of the short hull and prevent separation from the cylinder. Wake vortices will not be as synchronized and less excitation will result.

CFD runs were performed with 40 degree overlap to test this hypothesis. Figures 19 and 20 show the results for standard deviation and maximum Y/D. As expected, the amplitude is appreciably reduced for all headings, and particularly the hot spot is not as pronounced. We have not as yet validated these results with model tests.

CONCLUSIONS AND RECOMMENDATIONS

This study and the previous study both indicate that CFD may be used to successfully predict the occurrence of VIM. In particular, the "hot spots" for a particular spar configuration are identified and the amplitudes are conservatively estimated. The evidence is that the amplitudes may be more accurately predicted by refining the mesh, particularly in the area of the boundary layer. Furthermore, it may not be necessary to use a large number of nodes if the solver is capable of handling distorted element shapes. Run times are practical for engineering purposes. We have also found that modeling and meshing may be done fairly rapidly with available tools for 3-D drafting and automatic meshing.

At the moment CFD seems practical for looking into sensitivities in the early design phases. For example, CFD may be used to consider the relative affect of strake height and pitch and the impact of appurtenances. There is still not enough benchmarking work done to recommend that CFD should replace experiments for obtaining final design values, but as more studies are performed we believe this is a reasonable goal. In any event, as the MARNET study concluded [13], the application of CFD will require a specialized staff and rigorous application of "best practices" in modeling and solving of the problem. It will probably not be a tool in every engineer's toolbox, such as FEA has become, for example.

We recommend further work include:

1. Mesh sensitivities
2. Examination of the physical data other than gross responses, e.g.:
    a. Sectional forces (lift and drag of CFD vs. experiment)
    b. Structure of the wake
    c. Separation points
3. Different turbulence modeling

Finally, it is noted that all of the benchmarking described here was performed at model scale, Reynolds numbers between around 80,000 and 250,000. Full scale spars are at 30 million Re and higher. Some limited modeling of classic spars at full scale Reynold's numbers has been performed [14], however more correlation with full scale data is needed to validate both the CFD and the experimental results. CFD should be used in any event to study the physics of VIM scaleup to full scale Reynold's numbers.

REFERENCES

1. Vardeman, R.D., Richardson, S., and McCandless, C.R., 1997, "Neptune Project: Overview and Project Management," Proceedings Offshore Technology Conference, Houston, Texas, Paper Number OTC 8381.
2. Bangs, A. S., Miettinen, J. A., Mikkola, T. P. J., Silvola, I., and Beattie, S. M., 2002, "Design of the Truss Spars for the Nansen/Boomvang Field Development," Proceedings Offshore Technology Conference, Houston, Texas, Paper Number OTC 14090.
3. Finn, L. and Maher, J., 2003, "The Cell Spar for Marginal Field Developments," Proceedings Deep Offshore Technology Conference, Marseille, France.
4. Blevins R.D., 1990, Flow-Induced Vibration, Van Nostrand Reinhold, New York.
5. Mercier, R.S. and Ward, E. G., 2004, "Spar Vortex-Induced Motions Workshop – Proceedings", Offshore Technology Research Center, Texas A&M University, in preparation.
6. Magee, A., Sablok, A., and Gebara, J., 2003, "Mooring Design for Directional Spar Hull VIV," Proceedings Offshore Technology Conference, Paper Number OTC 15243.
7. van Dijk, R., Magee, A., Perryman, S., and Gebara, J., 2003, "Model Test Experience on Vortex Induced Vibrations of Truss Spars", Proceedings Offshore Technology Conference, Paper Number OTC 15242.
8. Irani, M. and Finn, L., 2004, "Model Testing for Vortex Induced Motions of Spar Platforms", Proceedings 23rd International Conference on Offshore Mechanics and Arctic Engineering, OMAE'04-51315, Vancouver, B.C., Canada.
9. Halkyard, J., Sirnivas, S., Holmes, S., Constantinides, Y., Oakley, O. and Thiagarajan, K., 2005, "Benchmarking of Truss Spar Vortex Induced Motions Derived from CFD with Experiments", OMAE 2005-67252, Halkidiki, Greece.
10. Atluri, Sampath *et al*: "CFD Simulation of Truss Spar Vortex-Induced Motion", Paper OMAE2006-92400, OMAE 2006 (June 2006)
11. Jansen, K. E., Whiting, C. and Hulbert, G. M., 2000, "A generalized-alpha method for integrating the filtered Navier-Stokes equations with a stabilized finite element method", Computer Methods in Applied Mechanics and Engineering.

12. Spalart, P. R. and Allmaras, S. R., 1992, “A one-equation model for aerodynamic flows,” AIAA 92-0439.
13. WS Atkins Consultants, “Best Practice Guidelines for Marine Applications of Computational Fluid Mechanics”, Report of the MARNET CFD project, 2003
14. Oakley, O., Constantinides, Y., Navarro, C. and Holmes, S., 2005, "Modeling Vortex induced Motions of spars In uniform and stratified flows", Proceedings 24th International Conference on Offshore Mechanics and Arctic Engineering, OMAE’05-67238, Halkidiki, Greece.

Run	Motion	T model [s]	T Full [s]
5	Roll	8.61	54.5
6	Pitch	8.5	53.8
7	Yaw	5.26	33.3
8	surge	25.3	160
9	Sway	25.5	161
11	Heave	3.87	24.5

Table 1 – Natural Periods of Model with Fours-Start Strakes

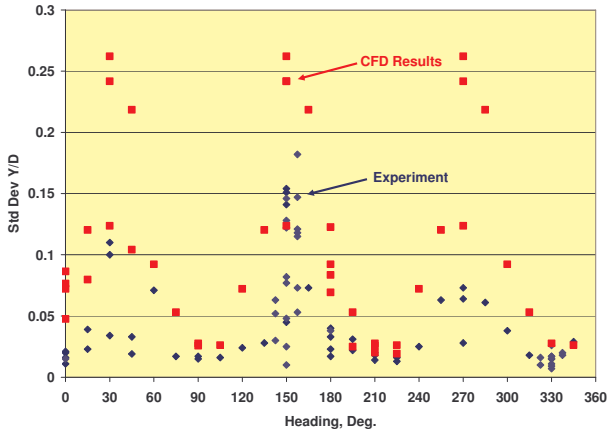

Figure 1 – Results from Three-Start Strake Study

Figure 2 – Spar Tested with Four-Start Strakes

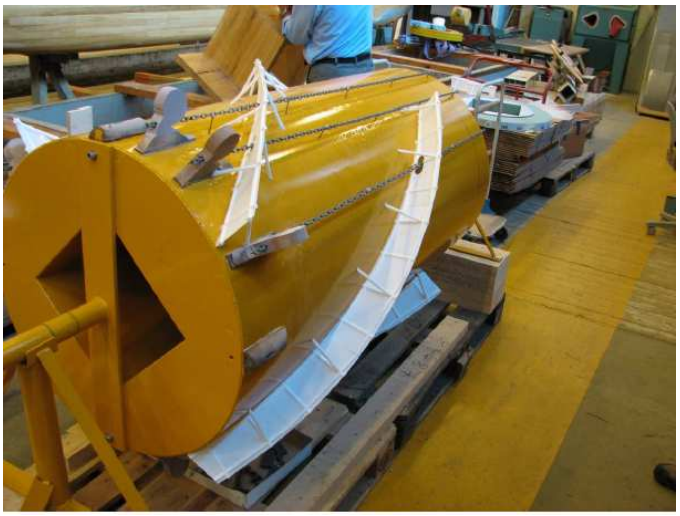

Figure 3 – Configuration A, Looking up from the bottom of the Hard Tank.

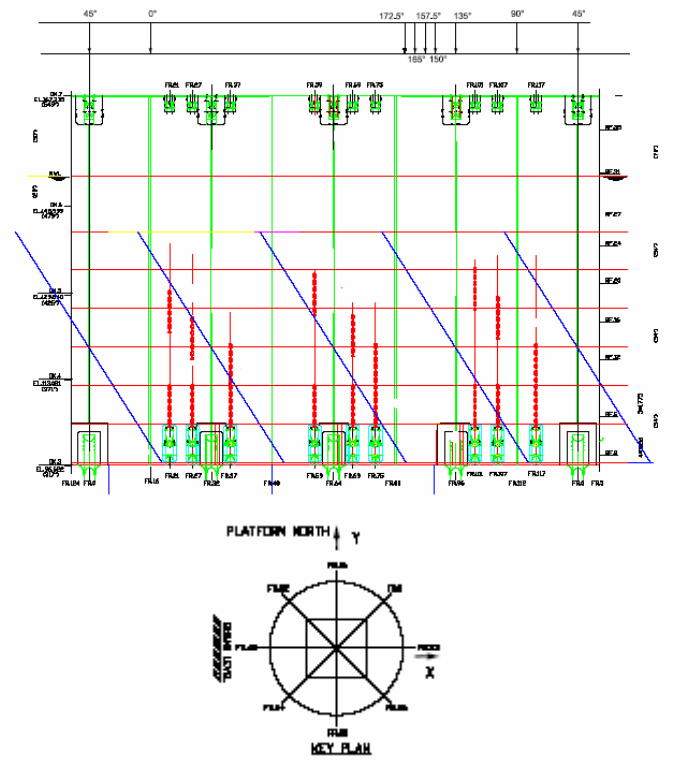

Figure 4 – Layout of Strakes and Chains

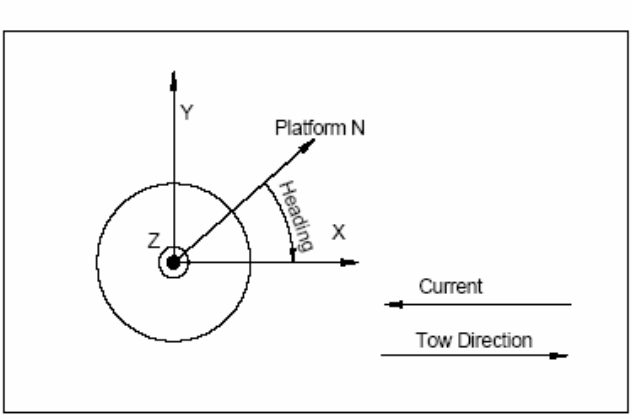

Figure 5 – Coordinate System

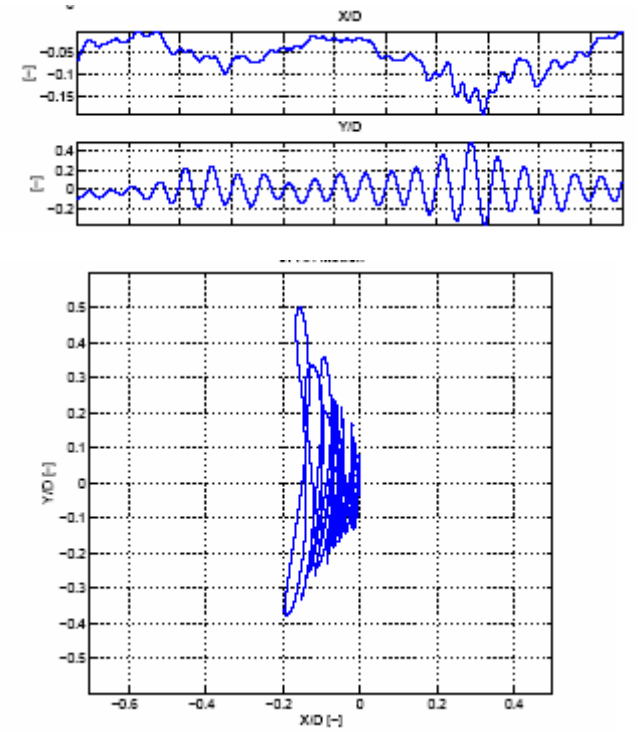

Figure 6 –Test Result (Conf. B, Ur 9, 240 Deg.)

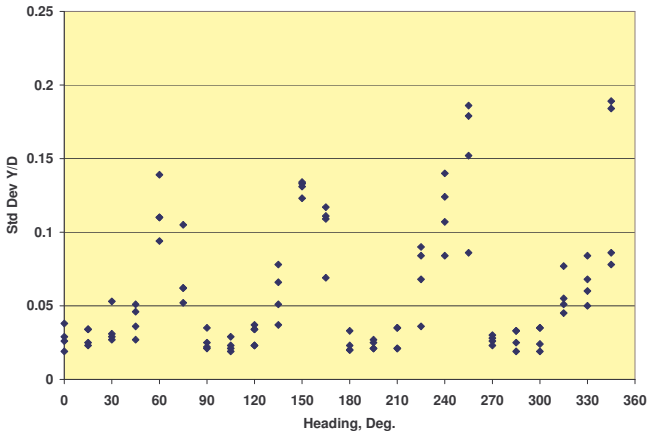

Figure 7 – Results for Configuration A

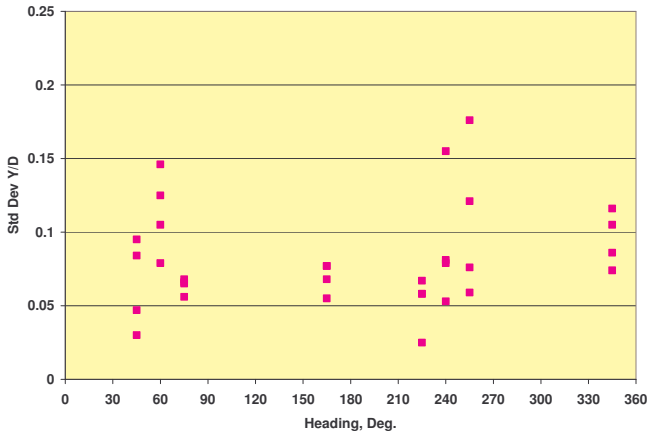

Figure 8 – Results for Configuration B

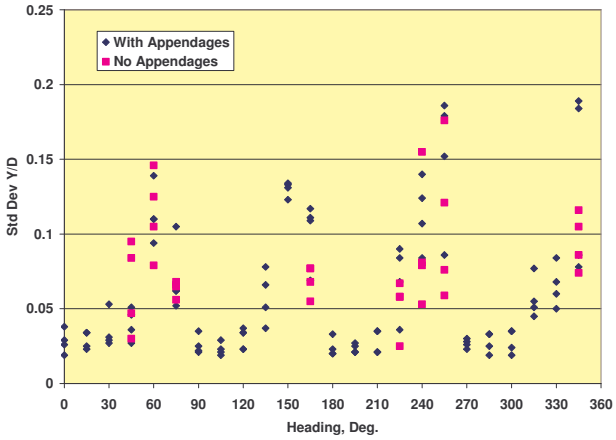

Figure 9 – Comparison of Responses with and without Appendages

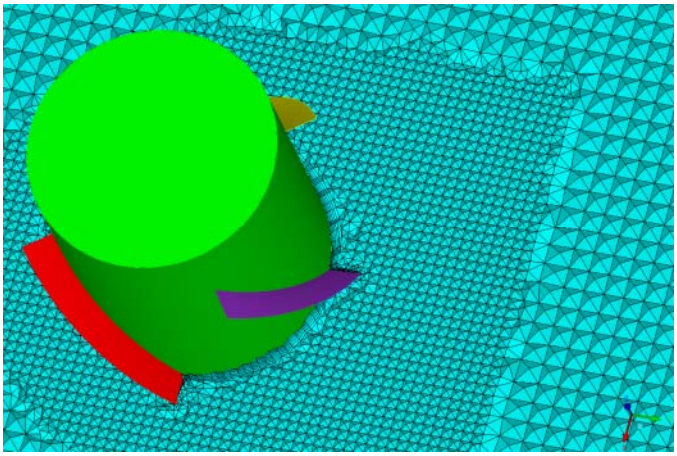

Figure 10 – Mesh A

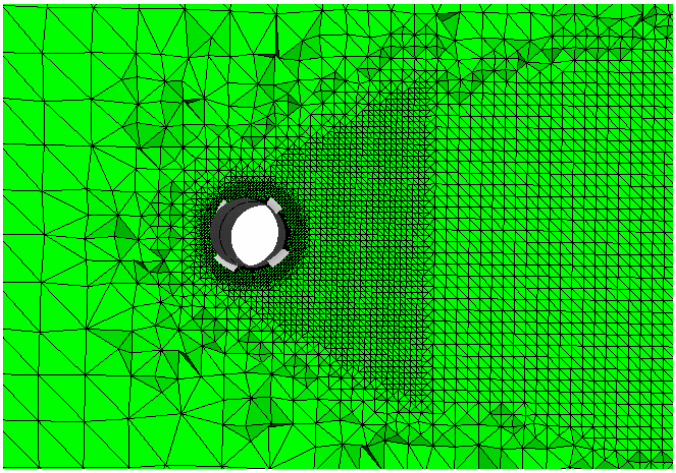

Figure 11 – Mesh B

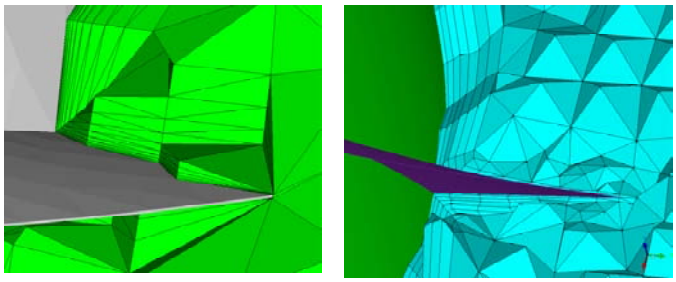

Figure 12 – Details in Boundary Layer of Mesh A (right) and Mesh B (left)

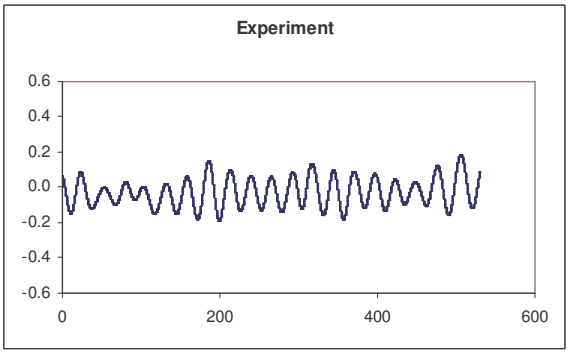

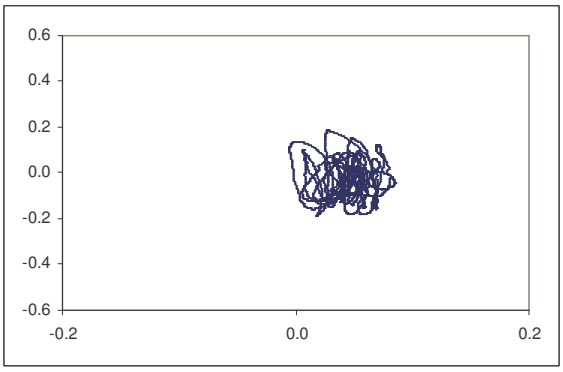

Figure 13 - Experimental Results for Ur 9, 225 Deg.

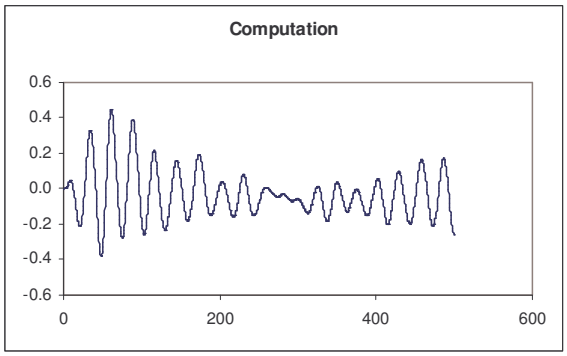

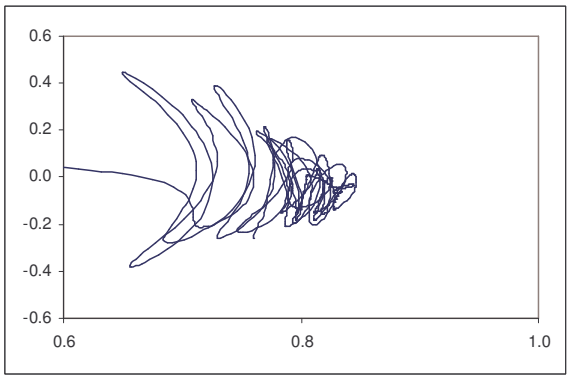

Figure 14 – CFD Results for Ur 9, 225 Deg.

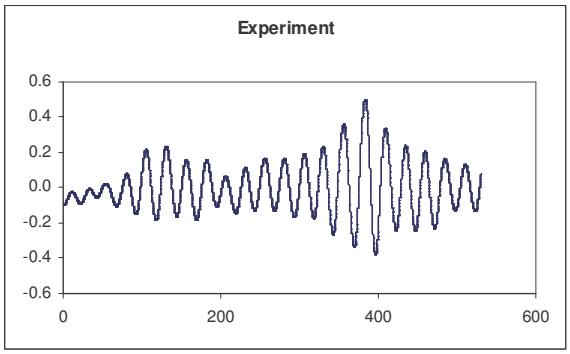

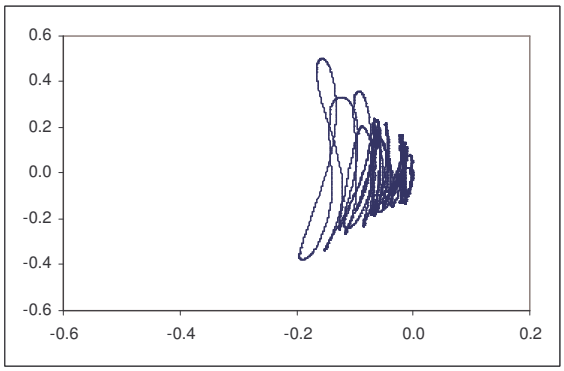

Figure 15 – Experimental Results for Ur 9, 60 Deg.

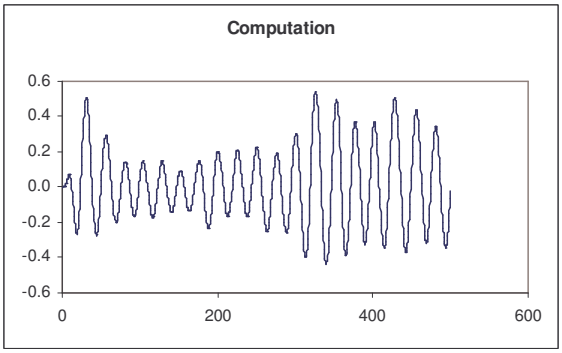

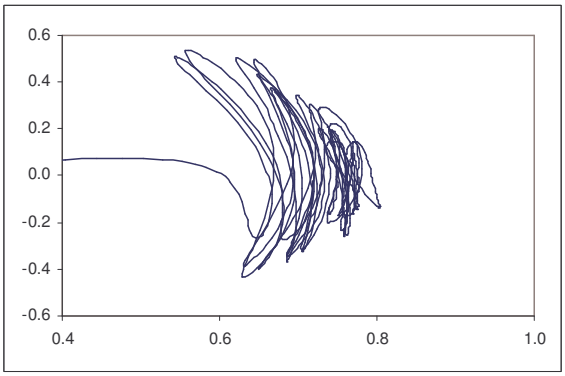

Figure 16 - CFD Results for Ur 9, 60 deg

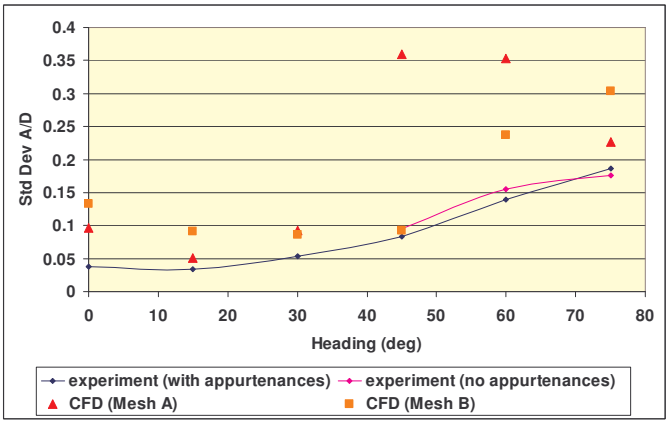

Figure 17 – Comparison of Four-Start Strake Experiments and CFD (Std Dev)

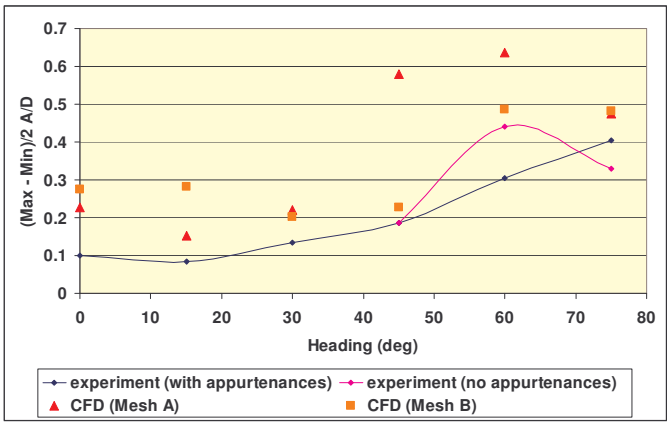

Figure 18 – Comparison of Four-Start Strake Experiments and CFD (Maximum A/D)

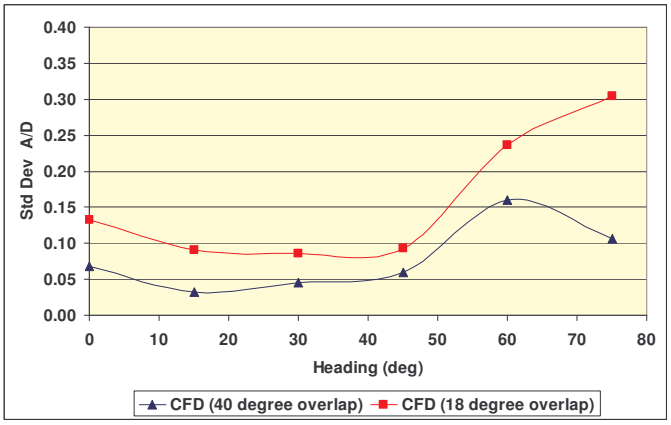

Figure 19 – CFD Results for 18 and 40 degree overlap (Std Dev)

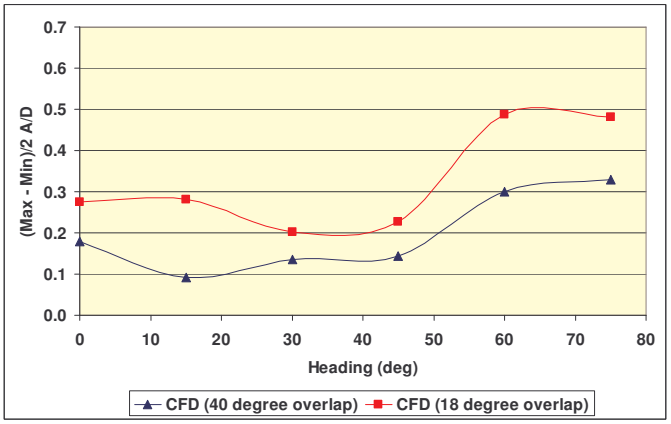

Figure 20 – CFD Results for 18 and 40 degree overlap (maximum A/D)